Proceedings World Geothermal Congress 2020+1
Reykjavik, Iceland, April - October 2021

Updated Shallow Temperature Survey, Resource Evolution and Preliminary Conceptual Geologic Model for the Coso Geothermal Field

Kelly Blake[1], Andrew Sabin[1], Mariana Eneva[2], Stephanie Nale[1], Michael Lazaro[1], Andrew Tiedeman[1], Dave Meade[1], Wei-Chuang Huang[1], David Fujii[3], Jade Zimmerman[1]

[1]Navy Geothermal Program Office, 429 E. Bowen Road, China Lake, CA 93555, USA, [2]Imageair Inc., 600 Greensburg Circle, Reno, NV 89509, USA, [3]T&E Technologies, 901 N Heritage Drive, Ridgecrest, CA 93555, USA

Kelly.blake@navy.ml; Andrew.sabin@navy.mil; meneva@imageair-inc.com; Stephanie.nale@navy.mil; Michael.lazaro@navy.mil; Andrew.tiedeman@navy.mil; david.meade@navy.mil; weichuang.huang@navy.mil; dfujii@epsilonsystems.com; jade.zimmerman@navy.mil

Keywords: Resource evaluation, Exploration, Coso Geothermal Field, Geology, Geophysics, InSAR

ABSTRACT

The Navy Geothermal Program Office completed a 2 meter temperature probe survey at and in proximity to the Coso geothermal field in 2019. This survey augmented our understanding of the larger shallow temperature anomaly associated with Coso and noted variations over time in the shallow ground temperature within the Coso field. These data were compared to other recently acquired data at Coso including a LiDAR lineation analysis and surface deformation measured with InSAR. A working hypothesis is that shallow temperatures, both directly above and proximal to the Coso geothermal field, have changed since the 1980s as the field has been produced and fluid levels have been drawn down. Specifically, within the Main Flank where the shallowest, longest running production has occurred within the field, the survey demonstrates a decrease in shallow temperature at present, compared to shallow high temperatures prior to production. Furthermore, the results of the survey demonstrate that the subsidence within the Main Flank detected with InSAR using satellite data, seem to coincide with this drop in shallow ground temperature. There may also be an increase in shallow temperature in the East Flank of the field that does not coincide with subsidence or inflation. This type of survey, paired with data sets that the Geothermal Program Office regularly analyzes, including microseismicity, will be collected in multiple phases to fill in data gaps and to achieve the most thorough representation of shallow temperatures within the Coso volcanic and geothermal field. Additionally, two of the largest earthquakes in the U.S. in the last 20 years occurred in early July of 2019 within the valley directly south of Coso, followed by numerous aftershocks. We analyzed the earthquake data recorded by the Coso seismic network for trends in the geothermal field and its surroundings, leading up to the M6.4 and M7.1 events on July 4 and 5, 2019, respectively. An overall deepening of regional seismicity was detected, as well as events at the northwestern end of the M7.1 fault rupture prior to either event. Interestingly, the Coso volcanic field experienced a non-detectable change in microseismicity around these historic events. Finally, in 2020, a conceptual geologic model of the Coso geothermal field was initiated using numerous data sets from the 30+ years of this actively producing field, as well as, roughly 40+ years of regional geoscientific work.

1. INTRODUCTION

The Coso geothermal field was the vision of a young geologic engineer, Dr. Carl Austin, who was hired to the United States (U.S.) Navy base at China Lake in 1961 to do explosives work. The nearby, poorly studied Coso volcanic field, with its myriad surface manifestations of an active hydrothermal system, caught his attention. Years of technical memos, publications, and outright battles, in addition to mapping and well drilling, ensued. On top of demonstrating to the scientific community that a geothermal resource might exist at Coso, Dr. Austin was also busy convincing the Navy that developing this resource would provide value to them. In 1975, the region was included in a Known Geothermal Resource Area (KGRA) by the U.S. Geological Survey (White and Williams, 1975). This opened the door for a one-time Bureau of Land Management (BLM) lease sale held in 1977 in which BLM withdrawn land (land withdrawn from the public domain for use by the Department of Defense) within the KGRA, inside the Navy base fence line, was available for geothermal leasing.

A 30-year development contract between the U.S. Navy and California Energy Company, Inc. was signed in 1979. The goal of this contract was to use private investor funding to develop Coso and to provide low-cost power from this resource directly to China Lake. By 1982, well drilling had proven that the resource was capable of producing 30 megawatts (MW) of power. A contract modification in 1986 allowed the contractor to sell the power to Southern California Edison, an electricity supply company in southern California, through the use of a Public Utilities Regulatory Policies Act (PURPA) contract; it was determined that the Navy was not authorized to wield power to itself as originally intended. In July 1987, Coso began delivering power to the California grid.

The Navy's nascent geothermal office (now Geothermal Program Office) at China Lake began exploring for utility-grade geothermal potential in the Coso Range long before the first development contract was signed. Cursory mapping, geophysical analyses and a temperature gradient survey, among other studies, began to outline the extent and temperatures of a large geothermal system. In addition to surface features, such as hot springs, fumaroles, travertine and sinter deposits, and hydrothermal alteration, the Coso volcanic field appeared to be very young, suggesting there may still be an active heat source (i.e., magma chamber) at depth.

At present, Coso has an installed capacity of 270 MWe, although it is currently producing below that level primarily due to the loss of fluid and pressure over time. A percentage of revenue from the sale of power derived from wells on the fee simple (Navy-owned) land remains for the Navy. Royalties from the sale of power on three existing BLM leases goes to BLM. The ratio of ~70:30 in

power sales has been supporting the Geothermal Program Office (GPO) and other Navy utility programs for more than 33 years. The GPO continues to sustain and improve upon acquired knowledge of the Coso reservoir through geologic, geophysical and engineering analyses.

2. GEOLOGIC SETTING

Coso occupies an area approximately 25 km^2 of the southwestern Coso Range of the northern Mojave Desert in the central part of eastern California. The Coso Range is located in the center of the KGRA, just east of the Sierra Nevada Mountains, Owens Valley to the north and the Indian Wells Valley to the south (Figure 1).

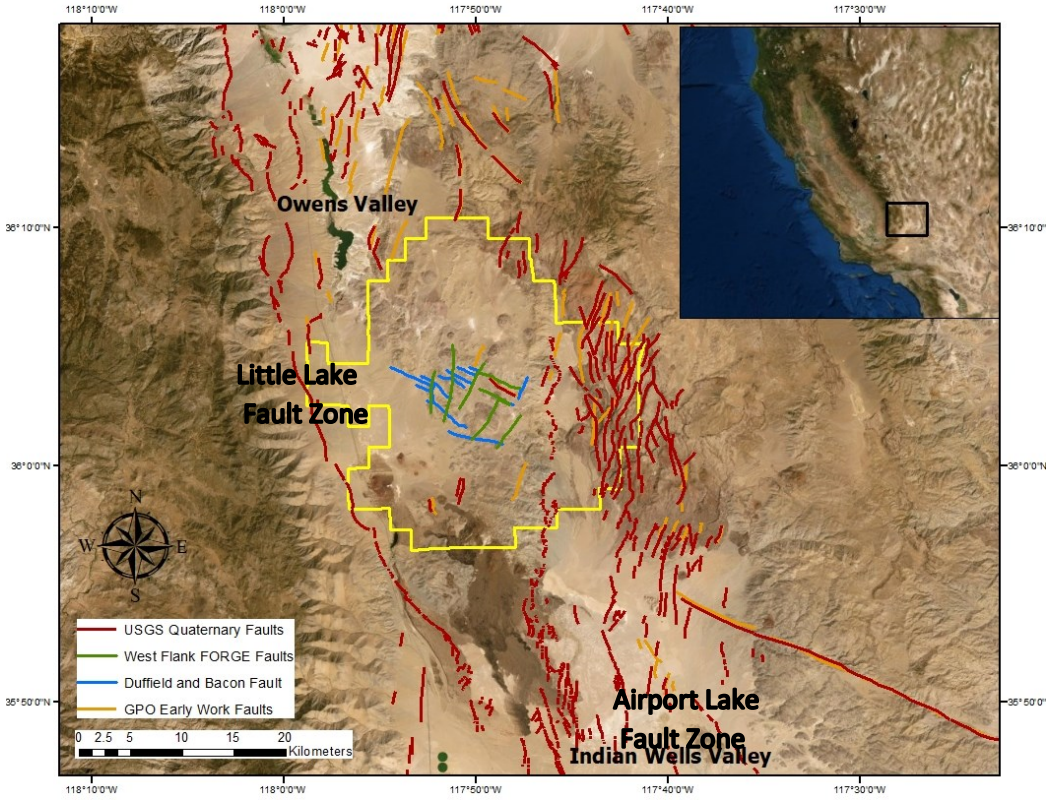

Figure 1: Known Geothermal Resource Area in yellow (KGRA) around the Coso volcanic field. Faults from multiple sources are mapped to demonstrate the structural setting of the volcanic field, within a step-over between the northwest striking Airport Lake Fault Zone to the south and the Little Late Fault Zone to the north.

Multiple types of data, in addition to production data, have been collected in an around Coso over the years to gain insight into this geothermal resource. Additional data sets are being collected and assessed in order to help characterize the evolution of the geothermal field since production began. This paper presents some of these recently collected and analyzed data in an effort to illustrate changes over time and then to place these changes in context after three decades of continuous production at the Coso geothermal field.

The Coso volcanic field (CVF) is a bimodal volcanic field of Pleistocene age comprised largely of rhyolite domes, rhyolite flows and their pyroclastic and epiclastic successions. Coeval basalt flows and cinder cones exist in the CVF but are volumetrically a minor part of the volcanic field (Duffield and Bacon, 1981; Duffield et al., 1980). Rhyolite domes range in age from roughly 700 ka to 60 ka reflecting more than 600 My of protracted dome growth in a relatively small (2.3 km^3) dome field (Simon et al., 2009). This magmatic system is maintained by the intrusion of basaltic magmas likely associated with ongoing deformation due to Basin and Range-style lithospheric extension (Duffield et al., 1980; Manley and Bacon, 1999). Shallow silicic magma chambers are the source of these rhyolites. A magma chamber is speculated to be located ~11 km beneath the Main Flank (Figure 2), based on an analysis of seismicity across the volcanic field, which demonstrates a shallowing of the brittle-ductile transition (Unruh and Hauksson, 2003). Conductive heating of the crust associated with the rhyolitic magma chamber is responsible for the elevated heat flow at Coso (Duffield et al., 1980).

The CVF rests unconformably on Mesozoic basement rocks composed of mafic and felsic, mixed complex intrusive rocks and granites. Basement rocks range from Cretaceous to Jurassic (Whitmarsh, 1998; Duffield et al., 1980) and host the geothermal field. Field relationships and age dating indicate that the granite intrusions are younger than the mixed complex intrusions (Monastero et al., 2005; Whitmarsh, 1998; Duffield et. al, 1980). Development drilling and logging indicates that the youngest rocks in the basement are aphanitic, felsic dikes that appear to be feeder dikes for the rhyolite dome field. Along the northwestern extent of the geothermal field, a set of NNE striking dikes serve as a barrier or at least a demarcation point, beyond which there are no productive portions of the field to the west (Sabin et al., 2016). The dikes are predominantly north-northeast striking and steeply dipping, and were intruded along pre-existing north-northeast-striking structures.

The tectonically active Coso Range is at the boundary between the Sierra Nevada (Sierran) microplate and the Basin and Range. The Sierran block moves 13 mm/year to the northwest with respect to the stable North American plate. Its motion is accommodated by

strike-slip and normal faulting in the Eastern California Shear Zone (called the Walker Lane in NV), a roughly 100 km wide zone of active deformation that terminates to the west along the Sierra Nevada (McCluskey et al., 2001; Unruh and Hauksson; 2003; Unruh et al., 2003; Roquemore, 1984). Springs, fumaroles, mud pots and regional alteration occurring within and along the eastern margin of the field are controlled by these strike-slip and normal faults.

The region is dominated by WNW to NW-striking dextral faults—the Airport Lake and Little Lake faults within the Indian Wells Valley and the Owens Valley, respectively—that step over to the right to the NW-striking dextral Owens Valley Fault Zone to the north. Coso is a horst block centered in this step-over with apparent pull-apart geometry (Figure 1). Relative uplift of the horst block appears to be controlled by NNE-striking E-dipping normal faults on the east side and NNW-striking, W-dipping faults on the west side. These faults, along with W-NW to NW-striking dextral-normal faults, step to the left, delineating the segmented and left-stepping geometry of a horst block.

The epicenter of a recent M7.1 earthquake near Ridgecrest, California occurred southeast of the Coso Range, in the Indian Wells Valley, and is centered on the Airport Lake-Little Lake fault system (Figure 1). Ongoing aftershock seismicity continues which defines these fault systems to the southeast and northwest of the CVF. Tectonic seismicity within the Coso geothermal field exists but is much reduced compared to the ongoing activity to the southeast and the northwest of the field after these large events.

3. RESOURCE EVOLUTION

Coso has been continuously operating for 33 years within the fence line of an active Navy weapons station, Naval Air Weapons Station, China Lake. In late 2009, a water augmentation project began pumping water to the Coso geothermal field from Rose Valley to the west. Throughout the last ten years, a greater understanding of fluid movement within the reservoir, natural recharge into the system and the effects of the augmented fluid has benefited the reservoir. Both the Navy GPO (resource owner) and the Coso Operating Company (COC, operators) continue to evaluate, analyze and interpret data from the field to assess the resource characteristics and the changes over time. Much of this work includes reservoir management and planning, with a significant focus on fluid management and injection strategy.

Data discussed were collected with the intent of aiding in reservoir management and planning, assessing subsurface fluid flow and the continued oversight of resource evolution. Figure 2 is a Digital Elevation Model (DEM) that was created from a LiDAR (Light Detection and Ranging) data set collected over the CVF in 2017. The three Coso areas identified on the figure are used as reference points in this paper: Main Flank, East Flank and Sugarloaf Mountain. For a full description of the data collection, lineament analysis and interpretation, see Blake et al. (2018). For the purposes of this paper, the LiDAR DEM and the lineations interpreted from the data set are compared to newly acquired, analyzed and interpreted data sets including two phases of a 2 meter temperature probe survey, InSAR (interferometric synthetic aperture radar) and seismicity.

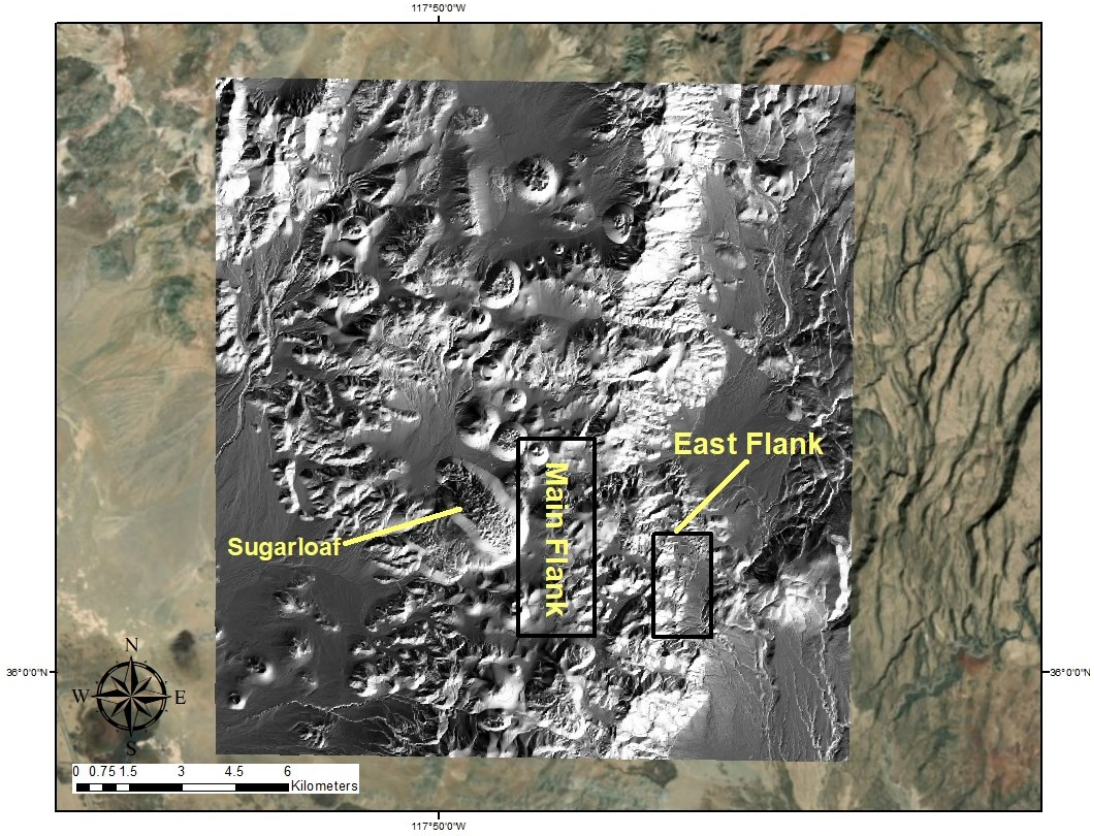

Figure 2: A DEM created from LiDAR data collected in 2017. The Main Flank, East Flank and Sugarloaf Mountain are marked as main points of reference.

3.1 2 Meter Temperature Probe

In June 2019, the GPO began its first phase 2 meter temperature probe (mtp) data collection within the CVF. The purpose of this phase of data collection was to compare the new measurements with previously collected shallow temperature data (Combs, 1980; LeSchack and Lewis, 1983; and Eneva et al., 2007). In September 2019, a second phase data collection was carried out to fill in gaps within the phase one data set, expand the survey and more thoroughly define observed anomalies. These data were collected to determine if they could, along with other newly acquired geologic/geophysical data sets within the volcanic field, provide insight into shallow temperature variation due to geothermal production.

Figure 3 includes results of both phases of the 2 mtp work and a lineament analysis of the LiDAR DEM (Blake et al., 2018). The highest shallow ground temperatures are proximal to areas of known surface manifestations in the eastern portion of the field (East Flank), the eastern area of the Main Flank and at the top of the Sugarloaf Rhyolite dome. Previous studies suggest that the East Flank area is reheating and, based on relatively young calcite veining, fluid pathways have been recently reactivated (Kovac et al., 2005). These conclusions, coupled with ongoing seismicity in the region (Section 4) suggests continued permeability evolution within the East Flank and therefore potential for changes in shallow heat flow. The shallow higher temperatures in the Main Flank are spatially associated with argillic hydrothermal alteration at the surface, but east of the main producing portion of the northern reservoir.

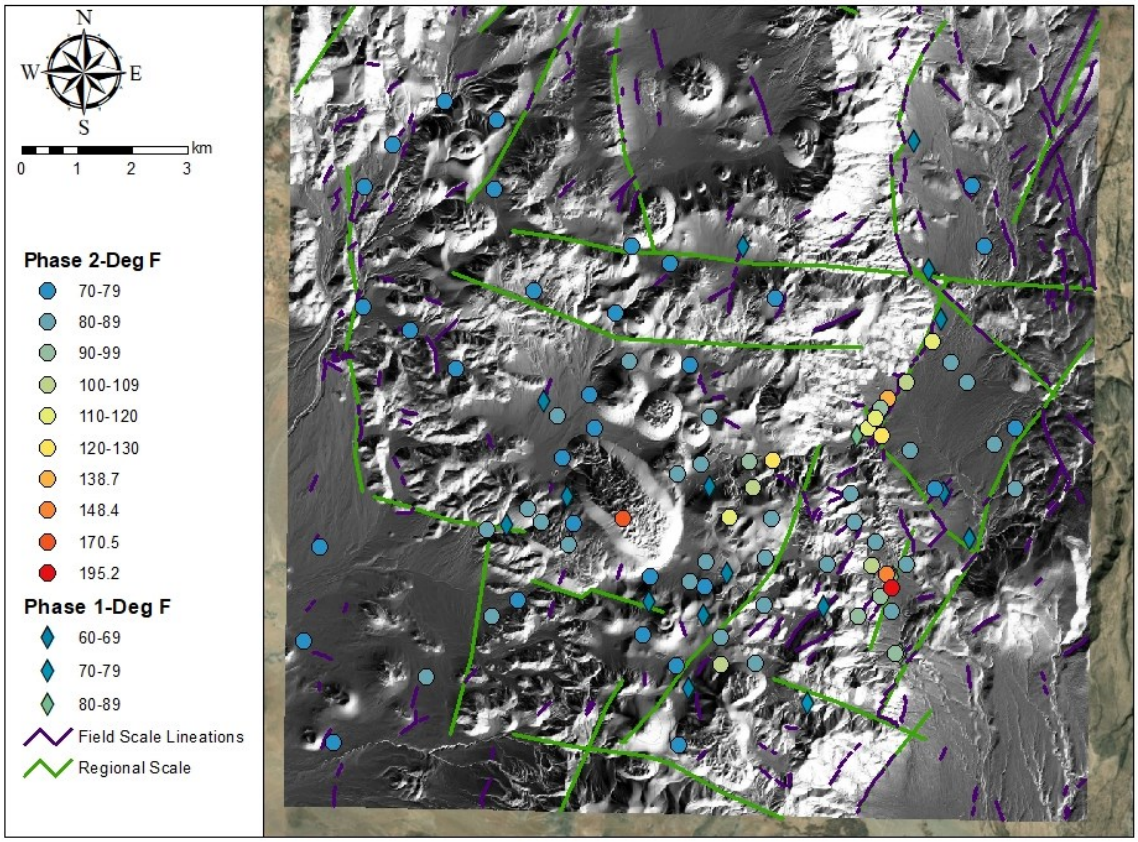

Figure 3: 2 mtp point locations and temperatures in Fahrenheit. The lineations and DEM are from LiDAR data analyzed, interpreted and discussed by Blake et al. (2018).

The collected data show that the shallow temperatures drop off significantly, as distance from these surface manifestations increases. The shallow temperatures on the eastern edge of the field have increased over the last two years (based on personal field observations), leading to a new fumarole in the East Flank, proximal to the hottest observed temperature 195.2°F (90.7°C). When comparing the shallow temperatures to the lineations identified from LiDAR interpretations, most fall along the identified lineations, however, within the Main Flank and East Flank, there are high temperatures that do not. The higher temperature points appear to follow the structural setting of the CVF, striking both in the NE and NW directions, which coincides with the strike of surface manifestations, as discussed in Section 2.

Figure 4 compares raw temperature core hole drilling data from the 1980s and 1990s with both phases of the 2 mtp survey, keeping in mind that the first phase measurements were taken purposefully near the temperature core hole locations. Of note, the near surface in the central northern Main Flank seems to show a decrease in shallow ground temperature when compared to the 500’ (152 m) contoured temperature. This difference can be explained with a decrease in production mass and an expanded steam cap in the central northern Main Flank. The shallow higher heat in the eastern Main Flank does not seem to correlate with temperatures at a 500’ depth, although this is likely due to a lack of core hole data in this location. Within the East Flank and the lineations to the north of the East Flank, the shallow heat seems consistent with the earlier temperature data set studied.

The observations seem to demonstrate shallow temperature variations over time, especially in the northern Main Flank, which is the shallowest portion of the reservoir continuously exploited for 33 years, and the East Flank, the youngest portion of the reservoir. Mapping of 2 mtp data in an active geothermal system may prove to be a useful and low-cost tool that informs shallow changes in fluid mass and fluid flow within a large and complex hydrothermal system.

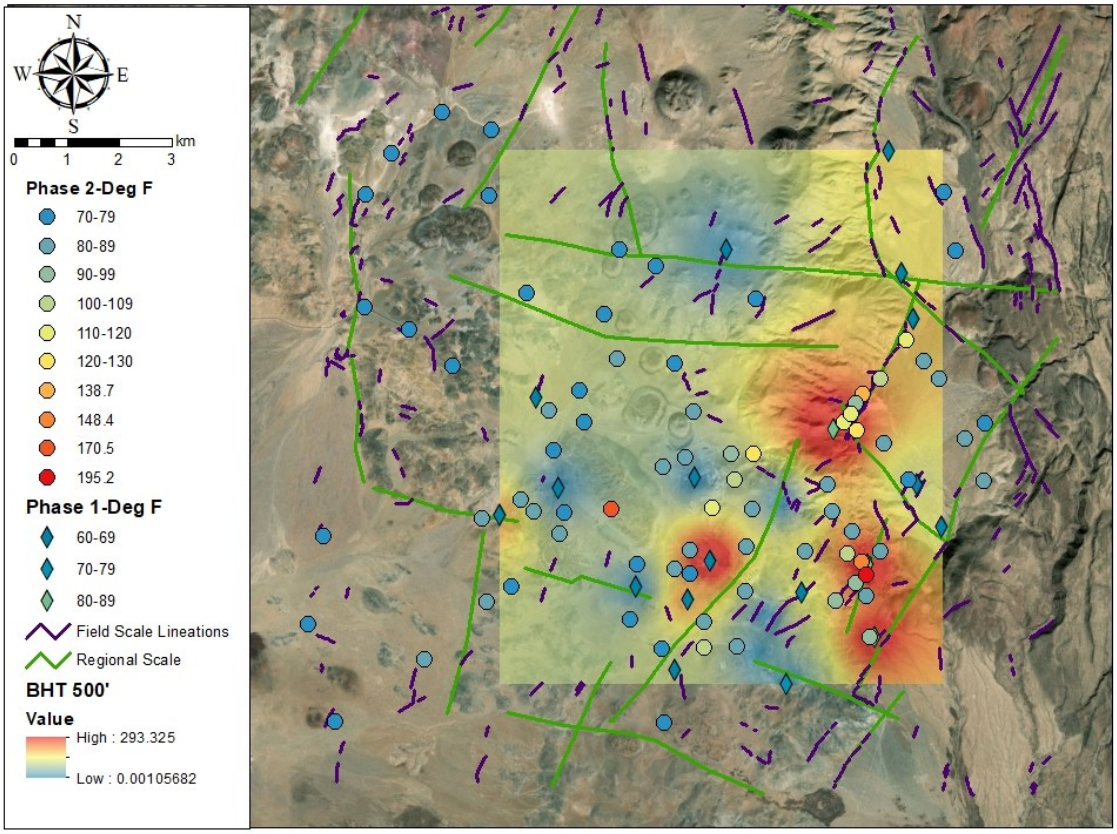

Figure 4: 2 mtp survey temperatures mapped together with contoured 500' temperature values from early temperature gradient drilling within Coso. The contouring was performed using the IDW method in ArcGIS.

3.2 InSAR

In addition to applying ground-based methods (e.g., leveling surveys, GPS), measurements of surface deformation can performed using InSAR data. Three earlier InSAR studies have analyzed several scenes at Coso from the 1990's (Fialko and Simons, 2000; Wicks, et al., 2001; Vasco, et al., 2002). These early studies suggested downward movements of the Earth's surface (subsidence) of up to 35 mm/year with a geothermal production zone depth down to 2.5 km.

We followed up these studies with InSAR processing of 203 scenes from two satellites, Envisat and Sentinel (Eneva et al, 2018), using a technique based on permanent and distributed scatterers (PS and DS), developed at TRE Altamira and known as SqueeSAR (Ferretti et al., 2011). The PS points can be buildings, well pads, points along roads and canals, fences, lamp posts, transmission towers, rock outcrops, etc. They serve as reflectors of the radar waves that are consistently identified in a sequence of radar scenes, so that time series of surface deformation are derived at each individual PS. The DS represent homogeneous areas emitting signals with smaller signal-to-noise ratios than the PS, but still significantly above the background noise. They include rangelands, pastures, and bare earth that are frequently encountered in relatively arid environments and rural areas.

Figure 5 shows three maps depicting vertical deformation rates from Envisat and Sentinel, as well as their difference at the Coso geothermal field. The SqueeSAR vertical displacements illustrated here are from two periods, February 2006 – September 2010 (Envisat) and January 2015 – April 2018 (Sentinel). Subsidence is represented with negative numbers in the figures, and uplift with positive numbers. The subsidence rate is lower in the Sentinel period, as shown in the difference map; the maximum subsidence from Envisat is 27.6 mm/year, while the maximum subsidence from Sentinel is 19.1 mm/year. The period of Envisat was prior to the addition of the augmented fluid from Rose Valley to the west of the volcanic field, whereas the Sentinel period overlaps with the period of augmented fluid and implemented subsequent injection strategy by Coso Operating Company.

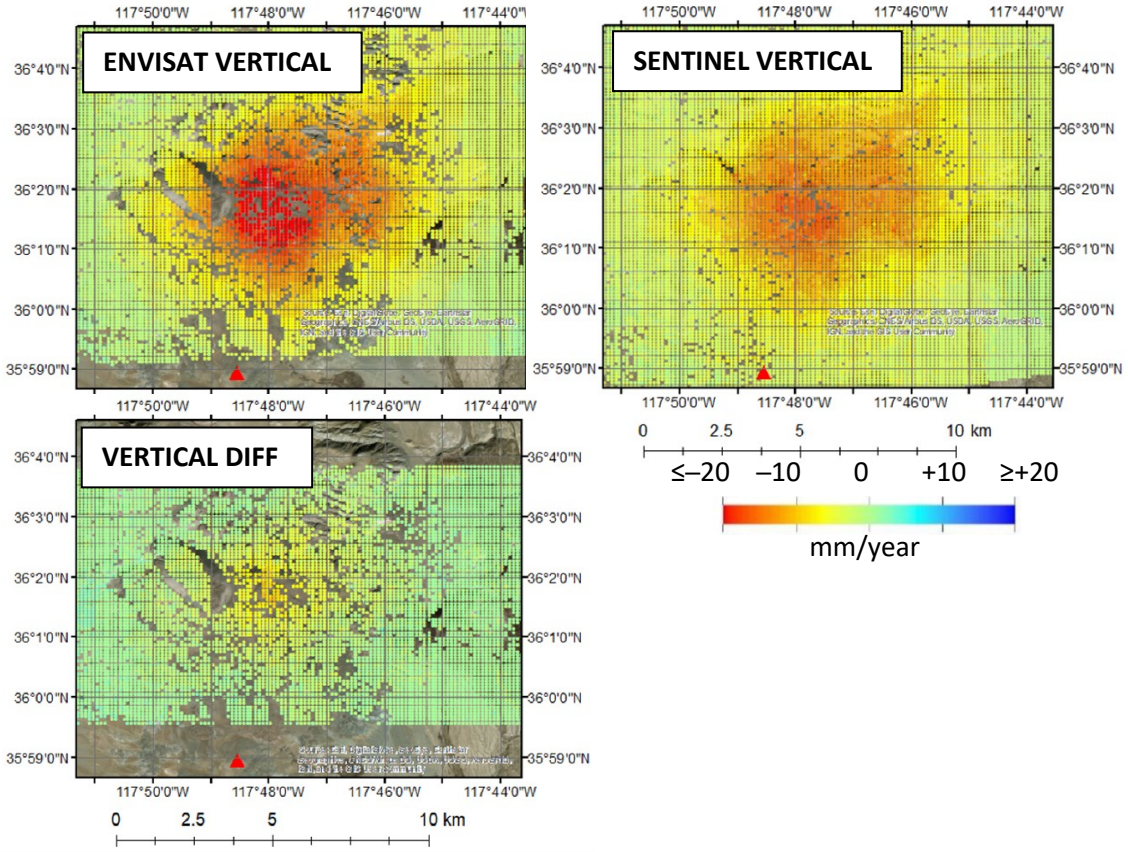

Figure 5: Maps of vertical surface deformation rates in 100-m pixels, as measured from Envisat and Sentinel, and their differences (Eneva et al., 2018). Vertical rates are color-coded according to color bar. Red triangle – location of a GPS station (COSO). Maps are superimposed on a satellite image from ArcGIS.

Figure 6 shows two profiles of interest, along which cumulative deformation is show in Figures 7 and 8. One of the profiles, A1-A2 in Figure 6, traces a lineament derived from LiDAR (Blake et al., 2018). It cuts northeast through the Main Flank, an area demonstrating a decrease in shallow temperatures from the 2 mtp survey. Gaps in the Envisat deformation progression (Figure 7) reflect lack of data in some parts of the profile. The Envisat period is 55 months long, and the duration of the Sentinel period is 40 months. The smaller maximum of cumulative subsidence in the Sentinel period, 58 mm, compared with 105 mm for Envisat, is partially explained by the different lengths of the two periods. However, if we take the rate of accumulation over 55 months for Sentinel, the maximum reached would have been ~80 mm, still smaller than that for Envisat. This is an expression of the reduced subsidence rate during the Sentinel period compared with the Envisat, seemingly due to the additional injected fluid and the injection strategy within geothermal operations. The other profile, B1-B2 in Figure 6, intersects the previous profile and passes through the area of maximum subsidence in a roughly perpendicular orientation of A1-A2. The maximum cumulative subsidence (Figure 8) in the Envisat period reaches 125 mm, and in the Sentinel period – 55 mm (~76 mm if the period were 55 months long), confirming the reduced subsidence rate compared with the Envisat period.

The observations, when paired with the LiDAR and the 2 mtp data, continue to demonstrate variation within the Main Flank of the CVF, likely due to the geothermal production. The location with the highest rates of subsidence correlates with a decrease in shallow temperature from 2 mtp; however, there is no notable change in surface elevation in the East Flank, where we have an increase in shallow temperature. Lastly, the orientation of the surface deformation, similar to the 2 mtp data, does tend to be consistent with the structural setting, striking both NW and NE (Figure 5).

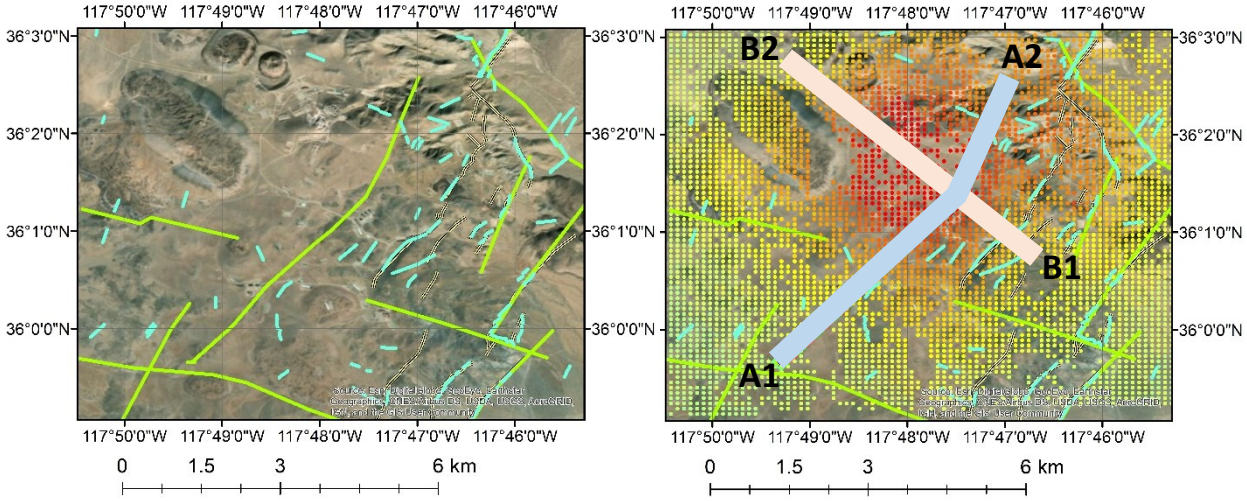

Figure 6: Maps showing lineaments based on LiDAR (left) and two profiles used in subsequent figures (right). Map on the right also shows vertical deformation rates from Envisat, color coded as in Figure 5. Profile A1-A2 traces the large lineament trending SW-NE. Profile B1-B2 from SE to NW passes through the Coso geothermal field through a known area of maximum subsidence. Both profiles are 200-m wide. LiDAR data from Blake et al. (2018).

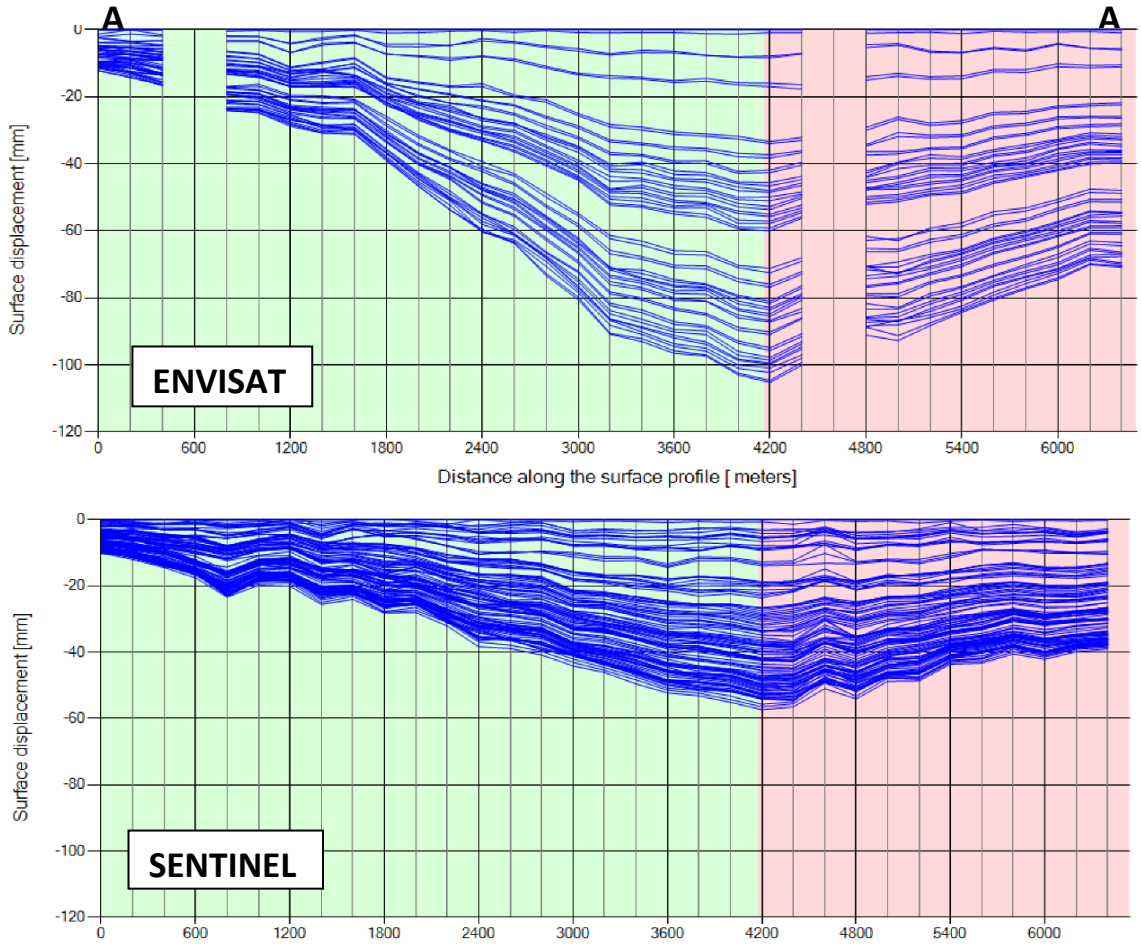

Figure 7: Cumulative deformation along profile A1-A2 in Figure 6, from Envisat and Sentinel as marked. Each line corresponds to a single satellite image. The two different colors to the left and right of the 4,200-m mark indicate the location where the profile changes direction.

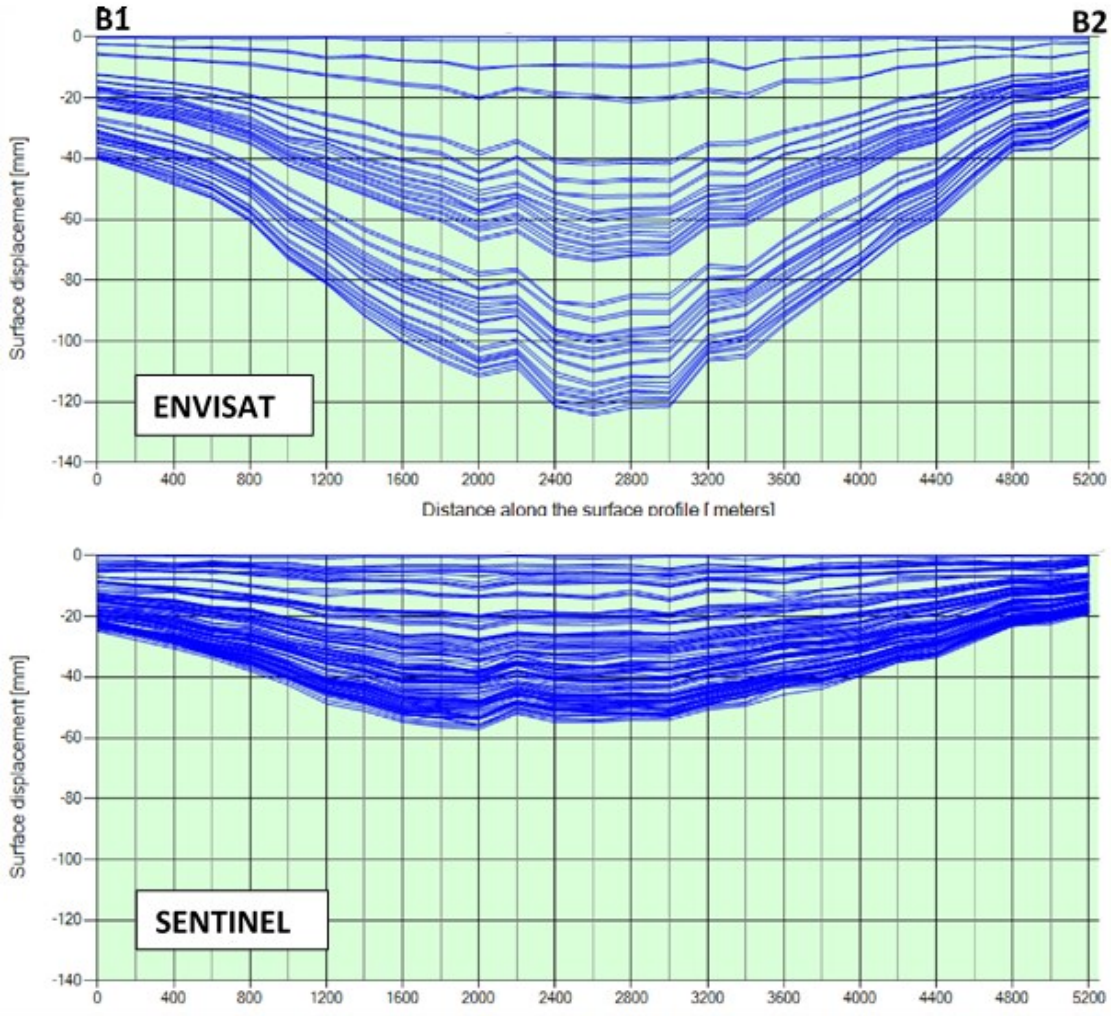

Figure 8: Cumulative deformation along profile B1-B2 in Figure 6. All notations like in Figure 7.

3.3 Discussion

Over the 30+ years of production at Coso, field evidence and remote sensing data indicate that the ground has measurably changed. This is likely a reflection of the resource evolving over time both naturally and, likely, a direct result of fluid and pressure decreases associated with production. In the last five years, the collection and analysis of LiDAR data, 2 mtp data and InSAR data suggests that localized subsidence and shallow temperature changes primarily in the Main Flank are associated with the drop in liquid levels within the reservoir itself. While this may have been predictable, especially to those aware that Main Flank wells were the largest producers at Coso, a refined application of this labor intensive but inexpensive 'tool' may be useful in assisting with fluid management and understanding the evolution of distal portions of this large geothermal field.

4. SEISMICITY IN THE COSO VOLCANIC FIELD, 2015 – 2019

Microseismicity in and around the CVF has been collected, analyzed and interpreted by the GPO since 1992, as well as studied by others in industry extensively due to the vast catalog (Mhana et al., 2019, Kaven et al., 2011). For the purposes of this study, we analyzed and interpreted seismicity trends from 2015 through mid-2019, discuss how it compares to the production and injection activity within the Coso Geothermal Field over the same period and briefly compare observations with the three data sets analyzed discussed in Section 3. Lastly, we investigate possible changes in seismicity as detected by our microseismic array leading up to the 2019 Ridgecrest earthquake sequence.

Over the four and a half years of data analyzed in this study, the seismicity of the Coso volcanic field increased from January 2015 – December 2016, with 1490 events within the month of December 2017 alone, the highest throughout the studied period (Figure 9). From that point on, seismicity begins an overall decreasing trend through November 2018.

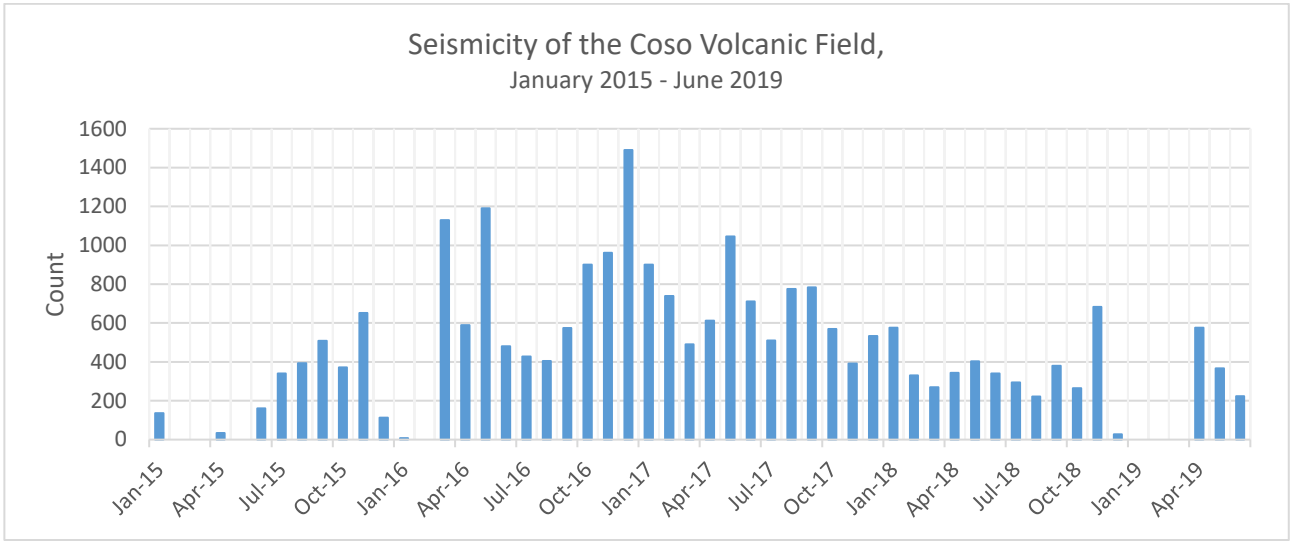

Figure 9: Monthly Coso seismic activity from January 1, 2015 – June 30, 2019.

Within the Coso geothermal field, there is a clear distinction between the Main and East Flank seismicity, with the East Flank being an area of known lower seismicity based on previous analysis. In the Main Flank, seismicity trends generally NW with a NE striking segment south of Sugarloaf (Figure 10). Seismicity in the SW edge of the Main Flank extends off in the northwest, slightly off strike from a majority of the seismicity within the Main Flank. Within the East Flank, the overall orientation of seismicity seems to be N-S with some extension along a NW-SE strike. These orientations of seismicity follow the structural setting of the CVF previously discussed.

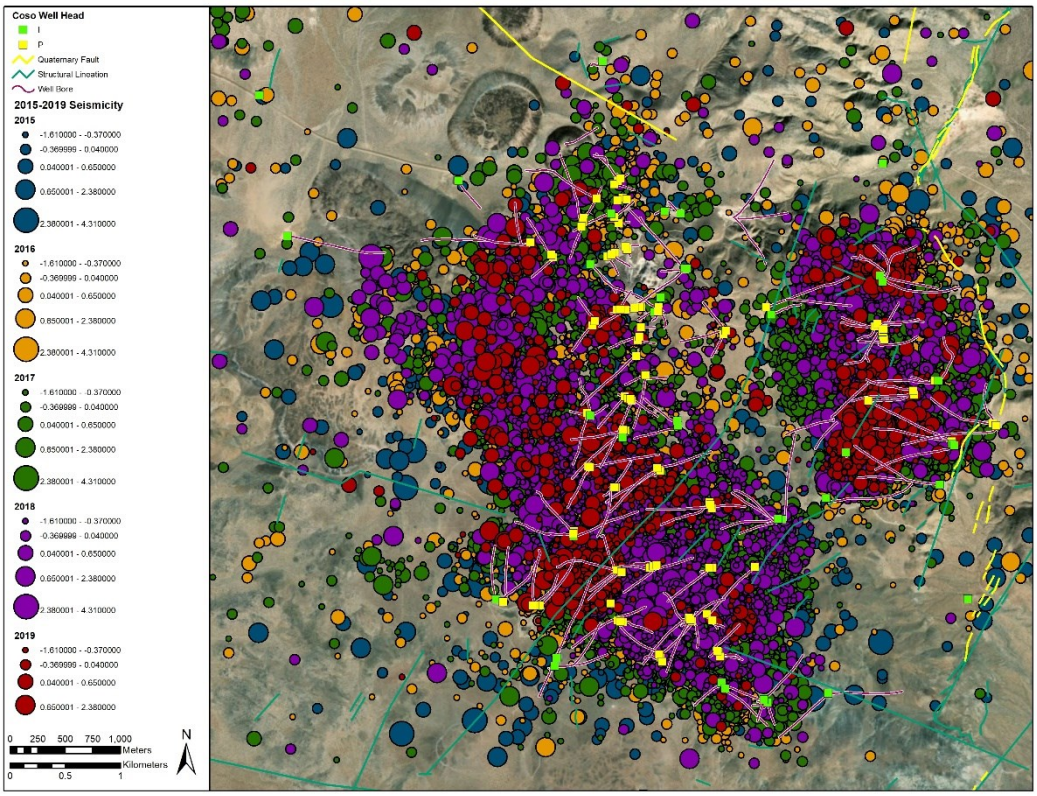

Figure 10: Seismicity within the Coso Geothermal Field 2015 – 2019 mapped with the injection and production wells, LiDAR lineaments and USGS Quaternary faults. Seismicity for 2015 (dark blue), 2016 (light orange), 2017 (green), 2018 (purple) and 2019 (red) are shown, scaled by magnitude.

Magnitudes of earthquakes within the CVF range from M-1.98 – M4.41 over the studied period (Figure 11). The majority of events (77%) have a magnitude less than zero, 21% are M0.0-1.0, and 0.3% of evens are M>3.0. In June 2015, a large number of earthquakes within the CVF were recorded at relatively large magnitudes for the area, M>3.5 – M<4.5. Locally, the largest earthquake in this sequence was M5.03 roughly 15 km northwest of the Coso geothermal area (Figure 12). This larger event occurred within the step-

over between the Airport Lake-Little Lake Fault Zones, but north of geothermal production, likely a product of tectonics as opposed to operation.

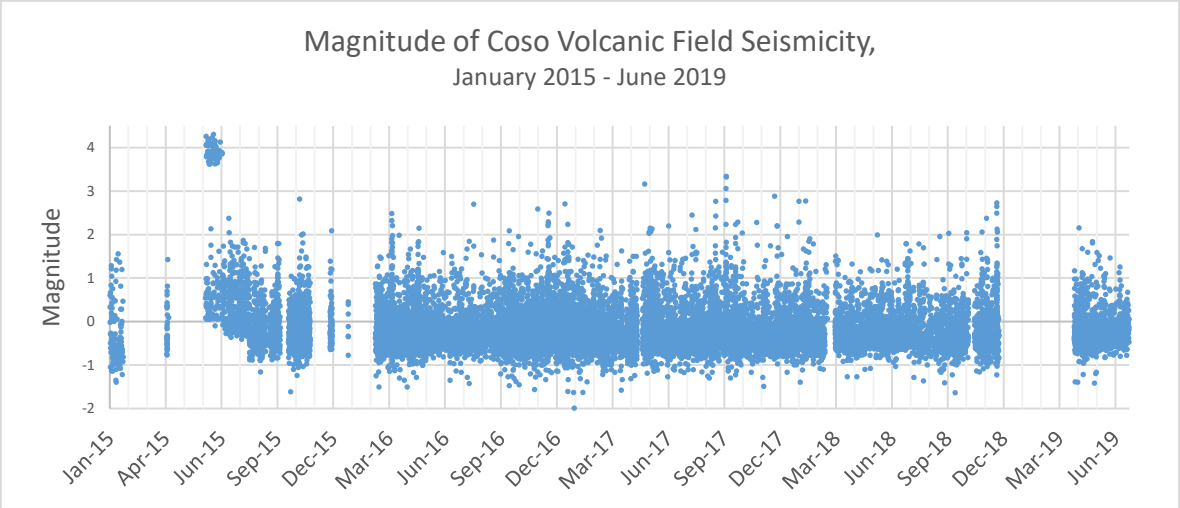

Figure 11: Magnitude of seismicity within the Coso volcanic field over time, from January 1, 2015 – June 30, 2019.

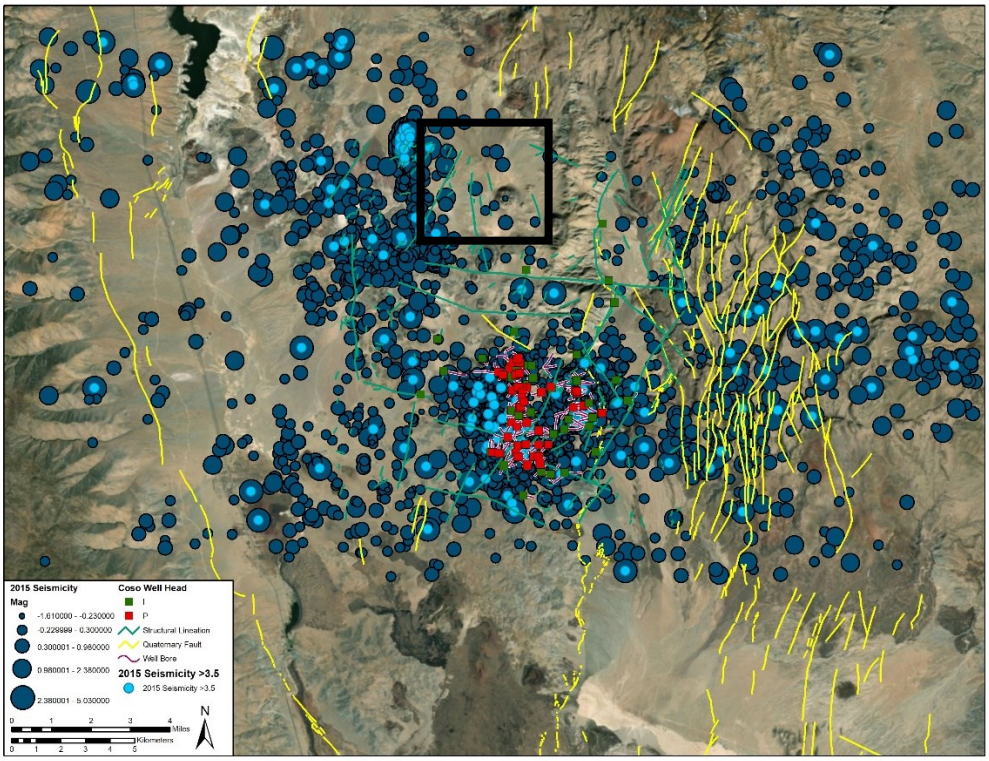

Figure 12: Map of the Coso volcanic field and surrounding area. Seismicity for 2015 (dark blue) are shown, scaled by magnitude. Events of M>3.5 are shown in cyan with a box around the location of the M5.03 in June 2015.

Since 2015, total production and injection at the Coso Geothermal Area was on a decline until mid-2017 when the trend of both production and injection rate steadied (Figure 13). Within the period studied, there are seasonal fluctuations to production and injection rates, as dictated by the conditions of the reservoir and injection strategy of Coso Operating Company (Figure 14). Within the four-year period June 2015 - June 2019, Coso seismic data seem to show a pattern of decreasing seismicity through the Winter – early Spring months, increasing trend through mid-Spring, decreasing again late-Spring through the early-Summer, and increasing seismicity through the Autumn months. The seismicity analyzed, although generally follows this trend, does not have the same distribution every year. Continued interpretation of these data are necessary to adequately determine correlation to production versus increased unrelated tectonic activity or regional fluid flow, although we do notice an increase in seismicity during well working events (i.e. well work overs and acid jobs) and will continue to monitor the propagation of seismicity relative to the wellbore.

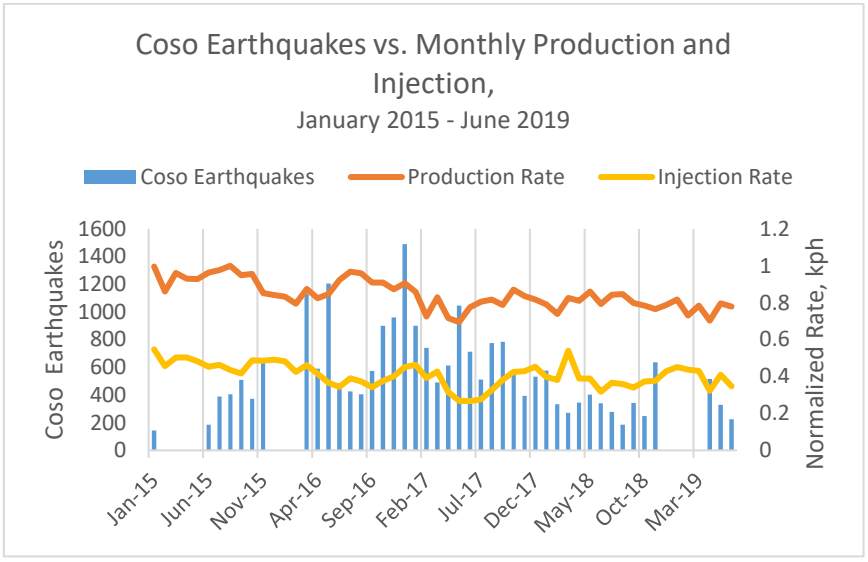

Figure 13: Monthly Coso seismic activity (blue) and total monthly normalized production (orange) and injection (yellow) rates (kph-thousand pounds per hour) from the Coso Operating Company between January 1, 2015 through June 30, 2019.

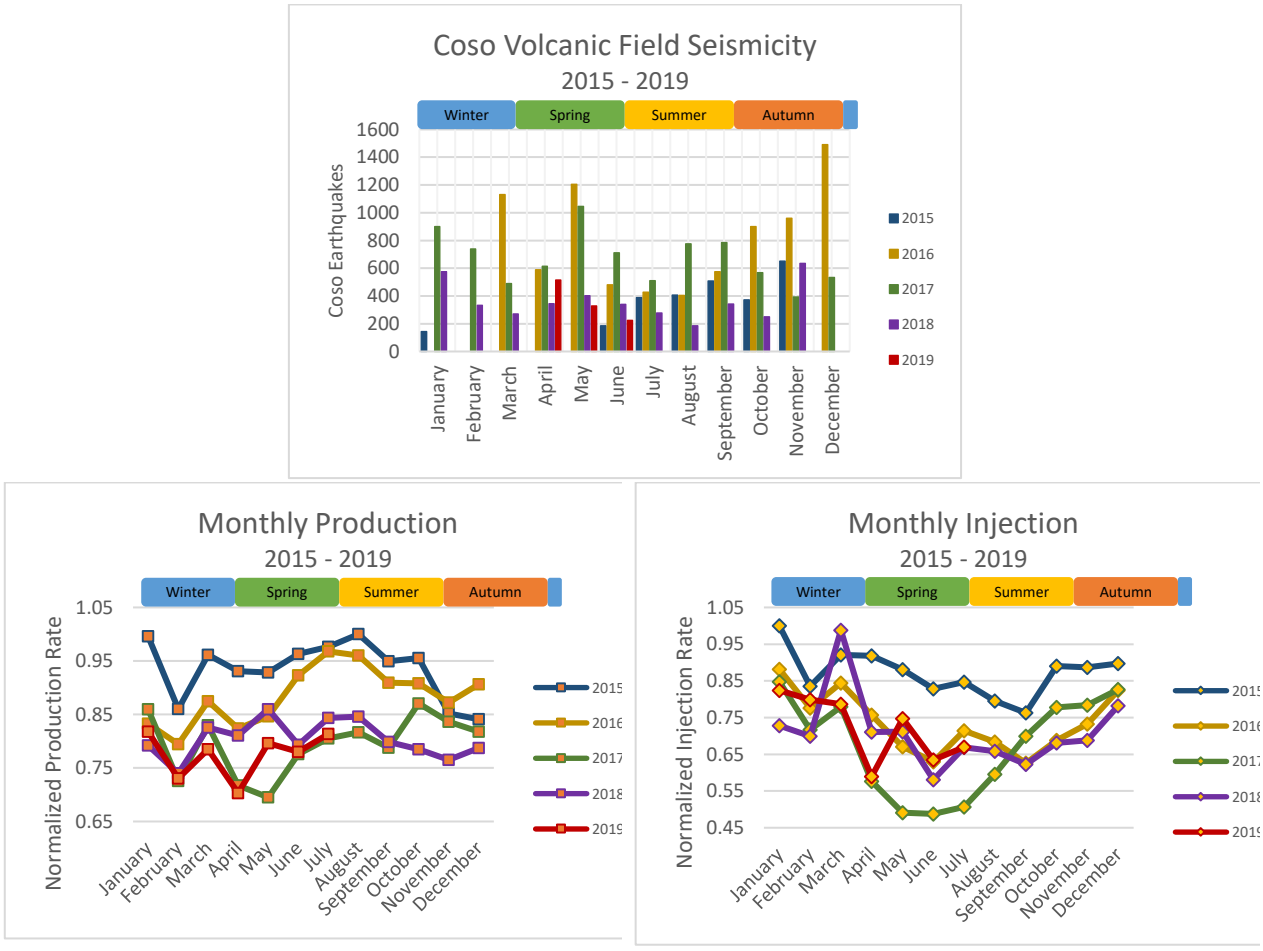

Figure 14: Total monthly normalized production (lower left) and injection (lower right) rates (kph) from the Coso Operating Company and Monthly earthquakes in the Coso volcanic field for years 2015 – 2019 (top), with seasons indicated.

The microseismic data, especially the representation in Figure 10, demonstrates the two main areas of the field, the Main and East Flanks, which coincide with (at least) two areas of upflow for the geothermal system and the two actively producing areas of the geothermal field. Lineations identified from the 2017 LiDAR data, also mapped on Figure 10, seem to correlate with gaps in the

microseismicity between the main and east flanks and/or areas with a change in the microseismicity trend. Further evaluation of how these two datasets correlate is necessary. The 2 mtp surveys performed in recent years have been skewed by the previously collected probe data and temperature core hole drilling, which were collected in the northern area of the CVF (Combs, 1980; LeSchack and Lewis, 1983; and Eneva et al., 2007). This lack of overlap does not lend itself to a comparison of these two data sets at this time, but is a likely future phase of the shallow temperature monitoring will expand to the south. The InSAR elevation change seen in Figure 5 seems to demonstrate a spatial correlation between microseismic events and the areas of subsidence, likely due to the production and injection of the Coso geothermal field over time. However, as the subsidence rate has decreased in recent years, we have yet to analyze a potential change in seismicity due to variation in the recent injection strategy.

4.1.Coso Seismicity Leading Up To The 2019 Ridgecrest Earthquake Sequence

On July 4 and 5, 2019, the Indian Wells Valley, just to the south of CVF, experienced 6.4 and 7.1 magnitude earthquakes respectively along the Airport Lake-Little Lake Fault Zones. The microseismic network at Coso is set up to accurately locate events within the geothermal field; however, we took a closer look at three months prior to these events to determine if our data demonstrated any variation in seismicity trends leading up to these two historic earthquakes.

During the three months leading up to the M6.4 and M7.1 earthquake sequence, seismicity within Coso was on an overall decreasing trend, even though production and injection rates were steady (Figure 15). During the same period, Figure 16 demonstrates seismicity migrating from clustering in the northern portions of the Main and East Flank in April to the southern portion of these two areas in May and June.

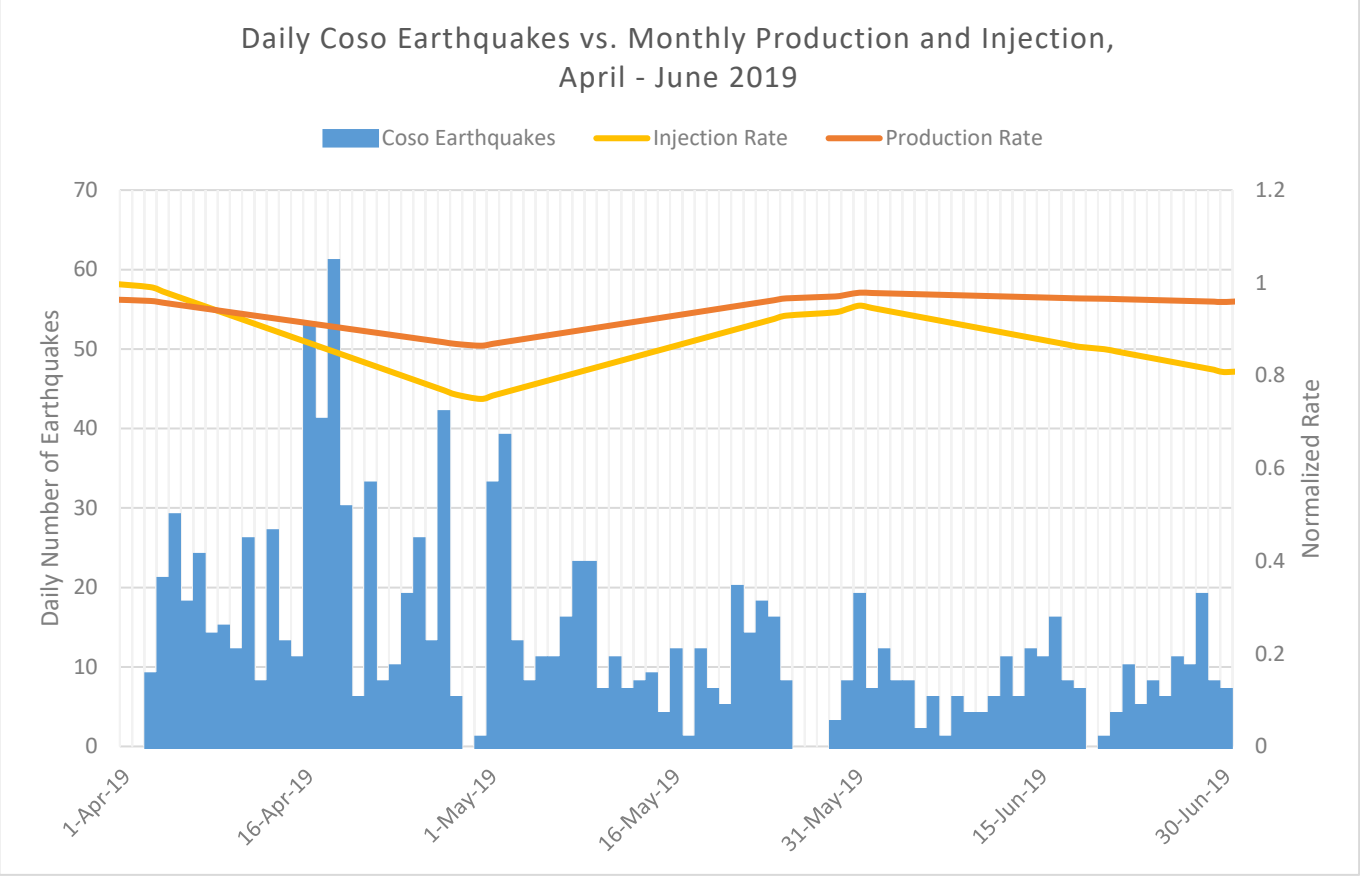

Figure 15: Seismicity within the Coso Geothermal Field between April and June, 2019 shown here with the normalized injection and production rates in the same time period.

The majority of the earthquakes within the three months studied were consistently M<0, with the second largest percentage in the M0 to M1 range; the largest Coso event measured in this period was M2.16 on April 11, 2019. This corresponds to a brief, but significant, increase in seismicity through mid-April, which correlates with a decrease in both production and injection within the Coso during a planned outage and subsequent change in operation of proximal wells and is unrelated to the Ridgecrest earthquake sequence.

Outside of the CVF, most of the seismic activity recorded on our array was located to the northwest and to the east (Figure 17). In the region surrounding Coso, deep events (4-6 km) had been increasing from 10% of seismicity in April, to 40% in May and 44% in June. In May and June, as demonstrated in Figure 16, seismicity did extend into the northern Airport Lake area, just south of the geothermal field, and, coincidentally, at the northern end of the main M7.1 rupture. No seismic activity was observed along the M6.4 rupture, the northeast striking fault in southern Indian Wells Valley, during the three months leading up to the event.

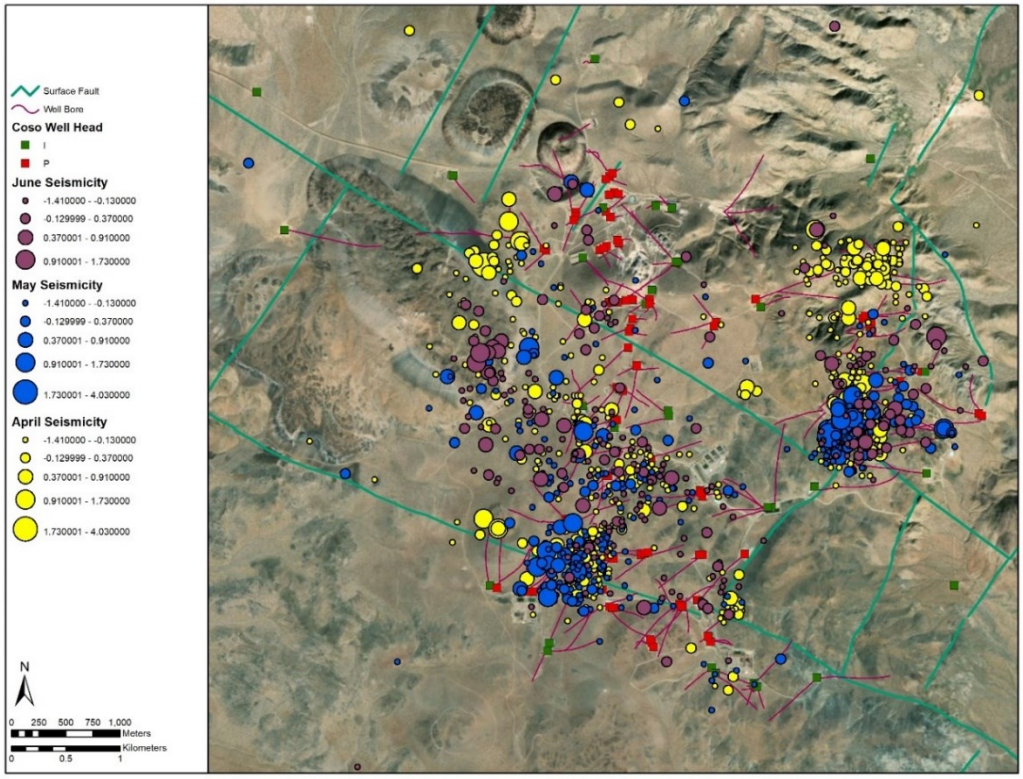

Figure 16: Seismicity within the Coso Geothermal Field between April and June, 2019 mapped with the injection and production wells and previously mapped surface faults.

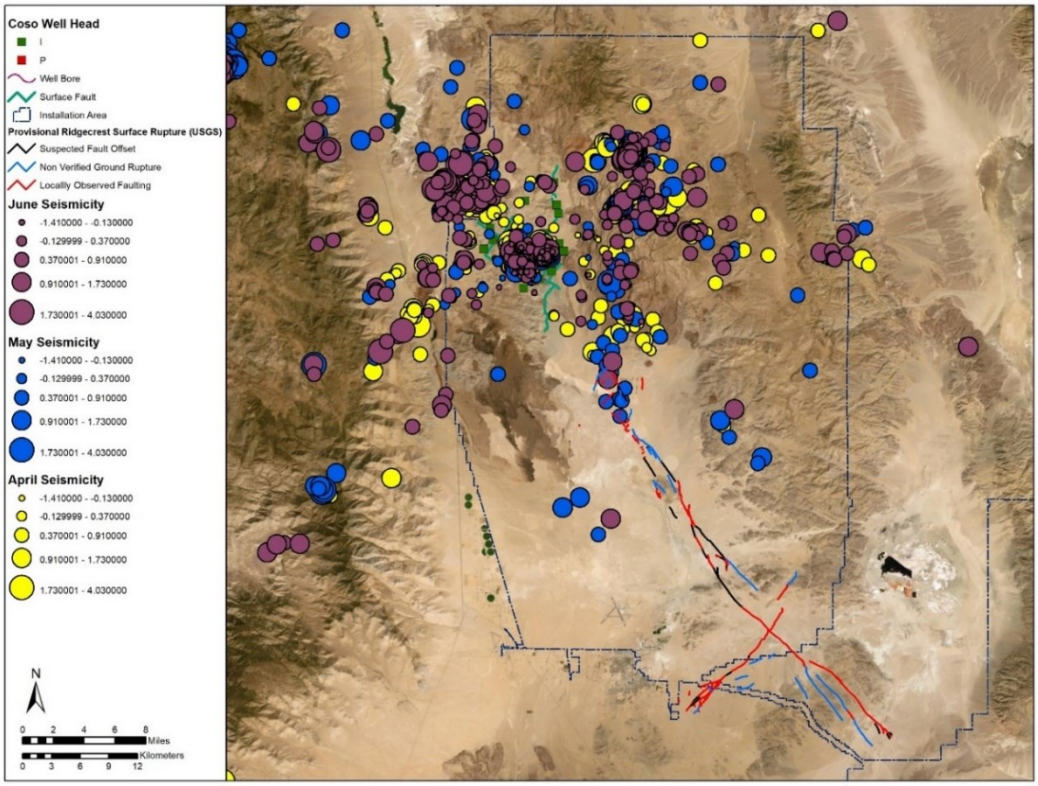

Figure 17: Seismicity from the Coso seismic network in the three months leading up to the large earthquake sequence that started on July 4, 2019. Along the rupture, there was some seismicity detected by the network at the northwest edge of the M7.1 rupture.

A decrease in seismicity between April and June, from the previous seismicity section, is on trend with the five-year analysis and cannot be correlated to the Ridgecrest earthquake sequence. Any variation in magnitude and depth observed during this three months period will need a denser statistical analysis to determine any correlation with the Ridgecrest sequence. GPO, in conjunction with numerous others, will continue to assess these two historic seismic events and any effects they may have on the Coso geothermal field.

Notably, the geothermal field never stopped sending energy down the transmission lines and the entire field was up and fully operational within 24 hours of the M7.1 earthquake. The faults within Coso did not slip enough to rupture the surface; however, there was some well-oriented erosional cracking along known Quaternary faults in the volcanic field. The aftershock sequences did not extend into the CVF and seemingly jumped this structural step over to the Little Lake Fault Zone from the Airport Lake Fault Zone. Continued analysis, interpretation and data compilation will occur in the coming months to years to fully understand this phenomenon.

5. CONCEPTUAL GEOLOGIC MODEL

In 2020, we began developing a conceptual geologic model for the Coso geothermal field, utilizing the large pre-existing data set from the 30+ year producing field and the 40+ years of geoscientific studies that had been performed. Models such as this have been put together numerous times throughout the long history of the Coso field and we intend to build on, and learn from, previous models as this model is developed and continuously updated bi-annually as funding allows.

We started with well heads, well traces, lithology, faults, temperature and seismicity. These are all datasets that are readily available, but do require a thorough quality check. To date, the majority of modeling time has been spent altering the rhyolite dike volumes after organizing and loading the data into Leapfrog Geothermal, Version 4.1.1 due to their intermittent and varied presence within logged cuttings.

The geologic model is 6.8 km in the north dimension and 7.5 in the east dimension and extends from the land surface, the highest of which is 3.4 m asl to a depth of -2.5 m asl. In total, the model is 300.9 km^3. The model currently has 11 lithologic units and 53 faults. The lithologic and fault data are constrained by geologic mapping and previous modelling work during the West Flank FORGE project (Siler et al. 2017, Whitmarsh, 1998, Duffield and Bacon, 1980). Well head, well trace, temperature and seismic data were all collected by downhole survey and, the later, from the microseismic array from the geothermal field maintained and analyzed by the Navy GPO.

The current representation of the lithology data, as seen in Figure 18 and 19, is of a simplified granitic basement with planar rhyolite dikes cutting through the subsurface, along strike with the current stress state based on drilling induced structures from image logs (Siler at al., 2017, Blake and Davatzes, 2011, Davatzes and Hickman, 2006, 2010). These dikes are modelled where they intersect the well from well cutting data and are modelled as feeder dikes for the rhyolite domes mapped at the surface. Differentiating between these rhyolite dikes to determine which are feeding each domes at the surface would take age dating work that has not been completed; we plan to apply recent surficial age dating work by the USGS to the model to best represent the volcanism as the model continues to develop. Other data sets we plan to incorporate are geochemistry, identified fractures/dikes from image logs and additional seismic events. This geologic model will inform an eventual reservoir model and continue to aid our understanding of the continued evolution of the Coso geothermal and volcanic field.

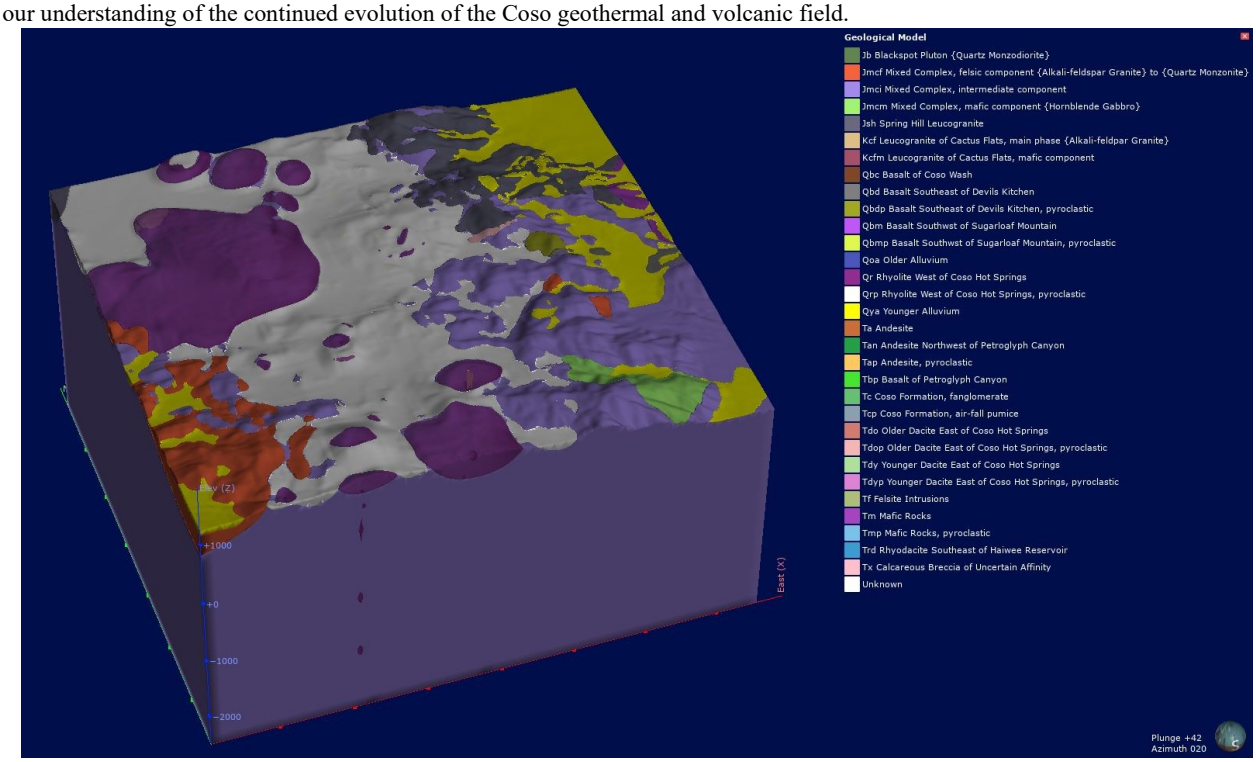

Figure 18: An angled image, with a view to the northeast, of the working 3D conceptual geologic model for the Coso Volcanic Field from the Leapfrog 4.1.1.

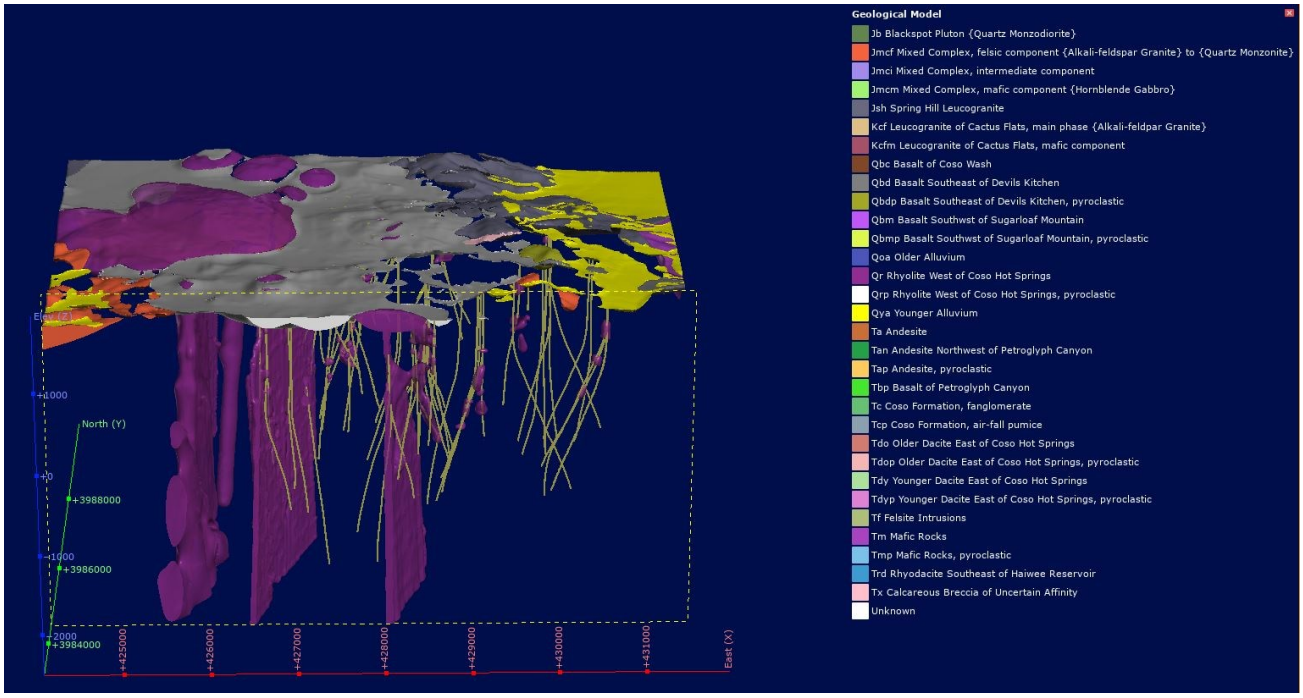

Figure 19: An image, with a view to the north and an east-west slice through the model, of the planar rhyolite dikes and well traces from the Coso Volcanic Field.

6. CONCLUSIONS

We demonstrate that GPO and COC have gained a greater understanding of the fluid flow through the reservoir and the effects of augmented injection. We are continuing to track the evolution of the Coso geothermal resource through geologic, geophysical and engineering-based studies. LiDAR, 2 mtp, InSAR and seismic data have provided opportunities to study this evolution separately and then synthesize these data sets to analyze both near surface and subsurface variations that have occurred within the Coso resource over the life of production. With the preliminary conceptual geologic model, a work in progress, we can continue to determine the utility of all these data to track, and eventually forecast, subsurface variation as it relates to production and injection.

Lastly, we will continue assess the effects of the Ridgecrest earthquake sequence on the Indian Wells Valley and the Coso volcanic field over time. A general lack of notably seismicity within the geothermal area after two large seismic events is of interest and the response within the reservoir can serve as a useful proxy for future similar activity.

7. ACKNOWLEDGEMENTS

The Navy GPO would like to thank their many collaborators; there is no way to name all of them at this time. This does includes the continued collaboration with Coso Operating Company, specifically Chris Ellis and Cliff Buck. The InSAR portion of this paper reflects a study at Imageair Inc., funded by the California Energy Commission (GEO-16-003). TRE Altamira has carried out the SqueeSAR processing of satellite data. We would like to thank Dr. Ole Kaven at the USGS in Menlo Park, California for his continued seismicity guidance and Mike Hasting for his help with analyzing the Ridgecrest earthquake sequence.

REFERENCES

Blake, K., Sabin, A., Lazaro, M., Tiedeman, A., Meade, D., and Huang, W., "LiDAR Analysis over the Coso Volcanic Field, CA." *Geothermal Resources Council Transactions*, (2018).

Blake, K. and Davatzes, N., "Crustal Stress Heterogenity in the Vicinity of the Coso Geothermal Field," *Stanford Geothermal Workshop*, (2011).

Combs, J., "Heat Flow in the Coso Geothermal Area, Inyo County, California. *Journal of Geophysical Research*, https://doi.org/10.1029/JB085iB05p02411, (1980).

Davatzes, N. and Hickman, S., "Stress and Faulting in the Coso Geothermal Field: Update and Recent Results from the East Flank and Coso Wash, *Stanford Geothermal Workshop*, (2006).

Davatzes, N., and Hickman, S., "The feedback between stress, faulting and fluid flow: Lessons from the Coso Geothermal Field, CA, USA," *World Geothermal Congress,* (2010).

Duffield, W.A. and Bacon, C.R., "Geologic Map of the Coso Volcanic Field and Adjacent Areas, Inyo County, California. U.S." *Geological Survey, Miscellaneous Investigation Series*, Map I-1200, (1981).

Duffield, W.A., Bacon, C.R., and Dalrymple, G.B., "Late Cenozoic Volcanism Geochronology, and Structure of the Coso Range, Inyo County, California," *Journal of Geophysical Research*, 85, B5, 2381-2404. (1980).

Eneva, M., Barbour, A., Adams, D., Hsiao, V., Blake, K., Falorni, G., and Locatelli, R., "Satellite Observations of Surface Deformation at the Coso Geothermal field, California." *Geothermal Resources Council Transactions*, 42, 1383-1401, (2018).

Eneva, M., Coolbaugh, M., Bjornstad, S., and Combs, J., "In Search for Thermal Anomalies in the Coso Geothermal Field (California) using Remote Sensing and Field Data," *Stanford Geothermal Workshop*, (2007).

Ferretti, A., Fumagalli, A., Novali, F., Prati, C., Rocca, F., and Rucci, A., "A New Algorithm for Processing Interferometric Data-Stacks: SqueeSAR," *IEEE Transactions Geoscience Remote Sensing*, 49(9), (2011), 3460-3470, (2011).

Fialko, Y., and Simons, M., "Deformation and Seismicity in the Coso Geothermal Area, Inyo County, California: Observations and Modeling Using Satellite Radar Interferometry." *Journal of Geophysical Research*, 105, 21781-21793, (2000).

Kaven, J.O., Hickman, S.H., and Davatzes, N.D., "Micro-Seismicity and Seismic Moment Release within the Coso Geothermal Field, California," *Stanford Geothermal Workshop,* (2011).

Kovac, K.M., Moore, J.N., and Lutz, S.J., "Geologic Framework of the East Flank, Coso Geothermal Field: Implications for EGS Development," *Stanford Geothermal Workshop,* (2005).

LeSchack, A and Lewis, J.E., "Geothermal Prospecting with Shallow-Temp Surveys," *Geophysics*, 48, 75-996, (1983).

Manley, C.R. and Bacon, C.R., "Rhyolite Thermobarometry and the Shallowing of the Magma Reservoir, Coso Volcanic Field, California," *Journal of Petrology*, 41, 149-174, (1999).

McCluskey, S.C., Bjornstad, S.C., Hager, B.H., King, R.W., Meade, B.J., Miller, M.M., Monastero, F.C., and Souter, B.J., "Present Day Kinematics of the Eastern California Shear Zone from a Geodetically Constrained Block Model," *Geophysical Research Letters*, 28(17), 3369-3372, (2001).

Mhana, N., Julian, B.R., Foulger, G.R., and Sabin, A., "Time-Dependent Seismic Tomography at the Coso Geothermal Area," *Stanford Geothermal Workshop,* (2019).

Monastero, F.C., Katzenstein, A.M., Miller, S.J., Unruh, J.R., Adams, M.C., and Richards-Dinger, K., "The Coso Geothermal Field: A Nascent Metamorphic Core Complex," *Geological Society of America Bulletin*, 177(11/12), 1534-1553, (2005).

Roquemore, G., "Structure, Tectonics, and Stress Field of the Coso Range, Inyo County, California," *Journal of Geophysical Research*, 85(B5), 2434-2440, (1984).

Sabin, A.E., Blake, K., Lazaro, M., Blankenship, D., Kennedy, M., McCullough, J., DeOreo, S.B., Hickman, S.H., Glen, J., Kaven, O., Williams, C.F., Phelps, G., Faulds, J.E., Hinz, N.H., Calvin, W.M., Ferretti, D., and A. Robertson-Tait, "Geologic Setting of the Proposed West Flank Forge Site, California: Suitability for EGS Research and Development," *Geothermal Resource Council Transactions*, (2016).

Simon, J.I., Vazquez, J.A., Renne, P.R., Schmitt, A.K, Bacon, C.R., and Reid, M.R., "Accessory Mineral U-Th-Pb Ages and 40Ar/39Ar Eruption Chronology, and their Bearing on Rhyolitic Magma Evolution in the Pleistocene Coso Volcanic Field, California," *Mineralogy and Petrology*, p.158, (2009).

Siler, D., Blake, K., Sabin, A., Lazaro, M., Meade, D., Blankenship, D., Kennedy, B.M., Mcculloch, J., DeOreo, S., Hickman, S., Glen, J., Kaven, O., Schoenball, M., Williams, C., Phelps, G., Faulds, J., Hinz, N., Robertson-Tait, A. and Pettitt, W., "The Geologic Framework of the West Flank FORGE Site," *Geothermal Resources Council Transactions*, (2017).

Unruh, J.R., Hauksson, E., Monastero, F.C., Twiss, R.J., and Lewis, J.C., "Seismotectonics of the Coso Range—Indian Wells Valley Region, California: Transtensional Deformation along the Southeastern Margin of the Sierran Microplate," in 'Glazner, A.F., Walker, J.D., and Bartley, J.M., Geological evolution of the Mojave Desert and Southwestern Basin and Range, Boulder, CO, GSA (2003).

Unruh, J. R. and Hauksson, E., "Seismotectonics of an Evolving Intra-Continental Plate Boundary, East-Central California," Geothermal Program Office Technical Symposium 8, University of California, Davis, CA, (2003).

Vasco, D.W., Wicks, C., Karasaki, K., and Marques, O., "Geodetic Imaging: Reservoir Monitoring Using Satellite Interferometry," *Geophysical Journal International*, 149, p. 555-571, (2002).

Whitmarsh, R.S., "Structural Development of the Coso Range and Adjacent Areas of East-Central California," PhD thesis, University of Kansas, (1998).

White, D.F. and Williams, D.L., “Assessment of Geothermal Resources of the United States,” *US Geological Survey Circ*. 726, (1975).

Wicks, C., Tatcher, W., Monastero, F., and Hasting, M., “Steady-State Deformation of the Coso Range, East Central California, Inferred from Satellite Radar Interferometry,” *Journal of Geophysical. Research*, 106, 13769-13780, (2001).